Optical integral field spectroscopy and *ROSAT* X-ray imaging of IRAS 09104 + 4109

C. S. Crawford[1]★ and C. Vanderriest[2,3]

[1]*Institute of Astronomy, Madingley Road, Cambridge CB3 0HA*
[2]*Observatoire de Paris-Meudon (DAEC), 92195 Meudon Cedex, France*
[3]*Canada–France–Hawaii Telescope Corporation, PO Box 1597, Kamuela 96743, Hawaii, USA*

ABSTRACT

We present results from a long observation using the integral field spectrograph ARGUS of the ultraluminous *IRAS* source IRAS 09104 + 4109, which is associated with the central galaxy of a rich cluster at a redshift $z = 0.44$. We map the distribution, kinematics and ionization state of its extended emission-line region, and show that both the nucleus and a secondary peak of line emission have ratios consistent with photoionization by a hidden, but luminous, quasar continuum. The kinematics of the ionized gas suggests that the galaxy and its extended emission-line region form a relatively static system at the cluster core. A strongly blueshifted component of emission-line gas around the nucleus reveals a central outflow, due either to a change in the central radio source, or to a massive supernova wind. We also present a ~ 30-ks *ROSAT* HRI pointed observation of IRAS 09104 + 4109. The X-ray image is extended, and a deprojection analysis confirms the presence of a 800–1100 $M_\odot$ yr^{-1} cooling flow in the $L_X = 2.9 \times 10^{45}$ erg s^{-1} cluster. A central dip is observed in the X-ray image, which may be caused by the outflow seen in the optical data. IRAS 09104 + 4109 is probably a very highly absorbed quasar, and presents the firmest case for a strong cooling flow occurring around a quasar, and the first to be discovered directly from an X-ray image.

Key words: galaxies: active – galaxies: clusters: general – cooling flows – galaxies: individual: IRAS 09104 + 4109 – quasars : general – X-rays: galaxies.

1 INTRODUCTION

IRAS 09104 + 4109 is one of the most luminous objects discovered by the *IRAS* satellite, and is identified with a cD galaxy at the centre of a rich, flattened cluster at $z = 0.442$ (Hutchings & Neff 1988, hereafter HN88; Kleinmann et al. 1988, hereafter K88). It has an optical spectrum character-istic of a Seyfert 2 galaxy, and a narrow-band image centred on redshifted [O III] resolves a secondary peak ~ 4 arcsec north of the galaxy core at position angle 25° (K88). The narrow emission lines are relatively broad, with a markedly blue-asymmetric profile. Although there are no broad com-ponents to the Balmer lines in the spectrum, there is plenty of evidence that IRAS 09104 + 4109 contains a powerful active nucleus. It has the most powerful radio source found associated with an *IRAS*-discovered galaxy, showing the strong core and double-lobed structure of a classical Fanar-off–Riley (FR) II (although its power at 1.4 GHz of $10^{24.5}$ W Hz^{-1} is borderline FR I/II; Hines & Willis 1993, hereafter HW93). In addition, the optical spectrum of IRAS 09104 + 4109 shows an ultraviolet excess, a highly polarized component (polarization of ~ 18 per cent, after subtraction of the stellar light), and a broad Mg II line (HW93). The scattered light continuum is characteristic of a low-luminosity QSO, although not one that is heavily red-dened. The large infrared (IR) excess of this source is thus probably produced by warm dust obscuring the active nucleus. The low ratio of nuclear-to-host luminosity (HN88; Soifer et al. 1996), and the lack of reddening and broad Balmer lines in the optical spectrum all suggest that this

★ Visiting observer, Canada–France–Hawaii Telescope, which is operated by the NRC of Canada, CNRS of France, and the Univer-sity of Hawaii.

dust is located between the broad- and narrow-line regions (HW93). IRAS 09104 + 4109 is different from other ultra-luminous *IRAS* galaxies, in that it is the only one known to be clearly located at the centre of a cluster of galaxies; also, unlike IRAS F10214 + 4724 (Eisenhardt et al. 1996) and perhaps IRAS F15307 + 3253 (Liu, Graham & Wright 1996), it shows no sign of being gravitationally lensed. Its IR spectral energy distribution is also markedly different from other ultraluminous galaxies, as it shows a strong peak over 5–60 μm (Frogel et al. 1989).

An *ASCA* spectrum of IRAS 09104 + 4109 revealed it as a powerful X-ray source, with a power-law-like spectrum and a strong line from helium-like iron (Fabian et al. 1994). A follow-up *ROSAT* High Resolution Imager (HRI) observation resolved the source as spatially extended, with a 0.1–2 keV (observed) luminosity of 2.9×10^{45} erg s^{-1} (Fabian & Crawford 1995, hereafter FC95). Given that IRAS 09104 + 4109 lies in a rich cluster, and the similarity of the (extrapolated) *ASCA* flux to that found by *ROSAT*, it is likely that the bulk of the X-ray emission is due to thermal bremsstrahlung. Indeed, the *ASCA* spectrum was better remodelled as an absorbed cooling flow, although the strength of the iron line could indicate a contribution from scattering of a hidden nucleus.

IRAS 09104 + 4109 is a particularly interesting source to study in detail, given the evidence for a strong QSO embedded in dust at the centre of a rich cooling flow cluster. Its immediate environment shows many fainter companion objects (over 11 within a 7.5-arcsec radius), which has also led to the suggestion that it is in the process of tidally interacting (HN88). In this paper we present two-dimen-sional spectroscopy of IRAS 09104 + 4109, allowing determination of the morphology, ionization state and kinematics of the whole emission-line system, with the aim of identifying the dominant processes occurring in and around this exceptional galaxy.

2 X-RAY OBSERVATIONS

IRAS 09104 + 4109 was observed with the *ROSAT* HRI for 21 868 s in 1995 April, and was added to the original pointed HRI observation (November 1994; FC95) to obtain a final X-ray image with a total exposure of 29 805 s. IRAS 09104 + 4109 is clearly detected, with 1375 ± 45 counts within a radius of 50 arcsec, after background subtraction and correction for vignetting. (1 arcsec corresponds to a projected distance of 7.5 kpc at the redshift of IRAS 09104 + 4109, assuming a cosmology of $H_0 = 50$ km s^{-1} Mpc^{-1} and $q_0 = 0$.) Converting directly from this count-rate (assuming a thermal spectrum) we deduce an 0.1–2 keV (observed) luminosity of $(2.89 \pm 0.11) \times 10^{45}$ erg s^{-1}, the same as our previously published value. The X-ray source associated with IRAS 09104 + 4109 is centred on the galaxy (Fig. 1), and its surface brightness profile is clearly extended beyond that expected from the HRI point-spread function (PSF) by several tens of arcseconds (Fig. 2). We have also extracted the X-ray surface brightness profile of the second brightest source in the field, which appears to fit the PSF of the HRI very well (Fig. 2), although this source contains only 66 ± 10 counts. Thus the extent of the X-ray emission of IRAS 09104 + 4109 is not an artefact of poor satellite tracking.
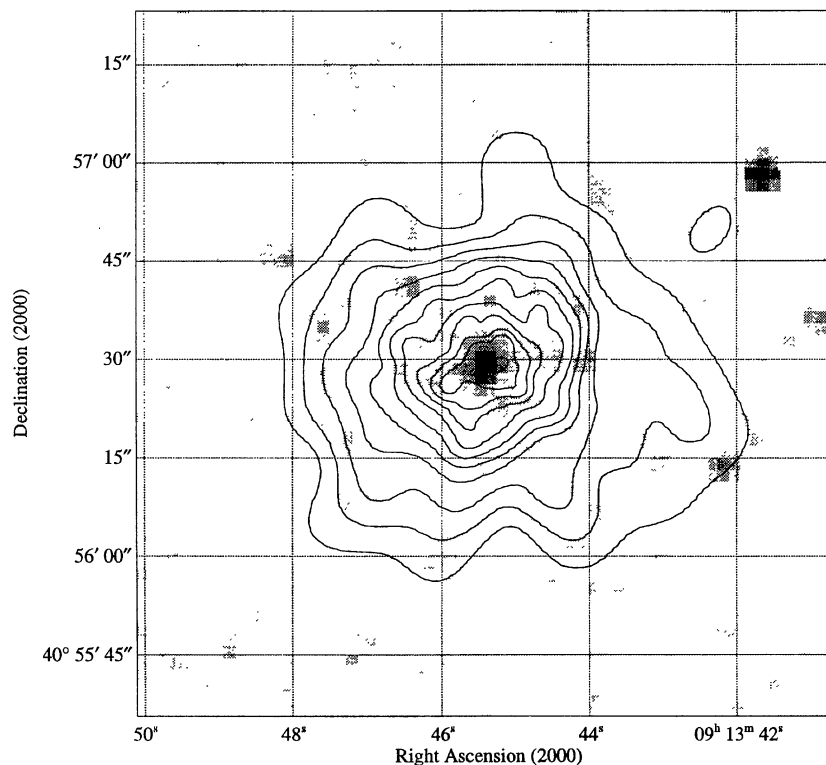

Figure 1. POSS image of IRAS 09104 + 4109 (grey-scale) overlaid with contours of X-ray emission. The X-ray image has been adaptively smoothed to have a minimum of 16 counts per smoothing bin (Ebeling, White & Rangarajan 1996), and the contour levels are 0.1, 0.14, 0.20, 0.28, 0.56, 0.79, 1.12, 1.58 and 2.24 counts per square arcsec. The central contour represents a dip in the X-ray intensity.

The surface brightness profile of IRAS 09104 + 4109 is fitted very well as a broken power law for radii over 2 arcsec; beyond a radius of 11 arcsec, the slope steepens from 1.1 to 2.5. Though less pronounced than that seen from the first 7.9 ks alone, the X-ray source still shows a dip at its centre in both the radial profile and the image (the most central X-ray contour in Fig. 1 represents a decrease to the second brightest contour level). We note that whilst the profile of the second source shows a similar structure at its centre, it is not significant.

Given the large spatial extent of this source (out to radii of 500 kpc), we can safely assume that the extended X-ray emission is due to thermal bremsstrahlung from the hot gas in the surrounding cluster. We deproject the surface brightness of the source into azimuthally averaged shells to make a radial emissivity profile. In combination with the assumptions of hydrostatic equilibrium and a gravitational potential for the cluster, it is used to derive the radial profiles of the physical parameters of the emitting gas, such as the density, temperature or pressure (Fig. 3). Deprojection is a standard technique for analysing the X-ray emission from clusters of galaxies, and we refer the reader to White (1996) and references therein for a detailed discussion of the technique and assumptions involved. The surface brightness profile is binned into shells of width 7 arcsec (to improve the signal-to-noise ratio, and to smooth out the central dip; 7 arcsec corresponds to 53 kpc). The absorption was fixed at the line-of-sight Galactic column density, 1.6×10^{20} cm^{-2}, as estimated from Stark et al. (1992). We assume a cluster velocity dispersion of ~ 1300 km s^{-1} (high, but consistent with the observed X-ray luminosity), core radius of 300 kpc, and the temperature of 11 keV measured by *ASCA* (CF95). (Values of 5 kpc and 300 km s^{-1} are used for the core radius and velocity dispersion of the central galaxy, but the solution is not highly dependent on the assumed potential of the galaxy, as this very central region is unresolved at the bin size used for the data.) The density and pressure of the gas within the core of the cluster are high ($P \geq 2 \times 10^{6}$ cm^{-3} K), and will thus be cooling rapidly. The cooling time is much less than a Hubble time at the age of the cluster; a cooling flow is taking place in the cluster, with an integrated mass deposition rate of ~ 800 M$_{\odot}$ yr^{-1} (Fig. 3). This rate increases to ~ 1100 M$_{\odot}$ yr^{-1} if we allow an excess column density of 2.5×10^{21} cm^{-2} at the redshift of the cluster, as fitted in the *ASCA* spectrum (FC95).

3 OPTICAL OBSERVATIONS

IRAS 09104 + 4109 was observed with the Canada–France–Hawaii Telescope (CFHT) during the night of 1995 January 8, using the integral field spectrograph ARGUS. ARGUS is an additional mode to the MOS-SIS double spectrograph, and uses a flexible bundle of optical fibres to transform independent spectra obtained over a $\sim 12.8 \times 7.8$ arcsec^2 hexagonal aperture into a pseudo-'long-slit' for collimation through the MOS (Vanderriest 1995; see also description in Crawford & Vanderriest 1996, hereafter CV96). Each fibre has a diameter of 0.4 arcsec.

The weather conditions were photometric, the seeing being typically 0.5 arcsec during the observations. Four consecutive frames were taken with the ARGUS aperture cen-
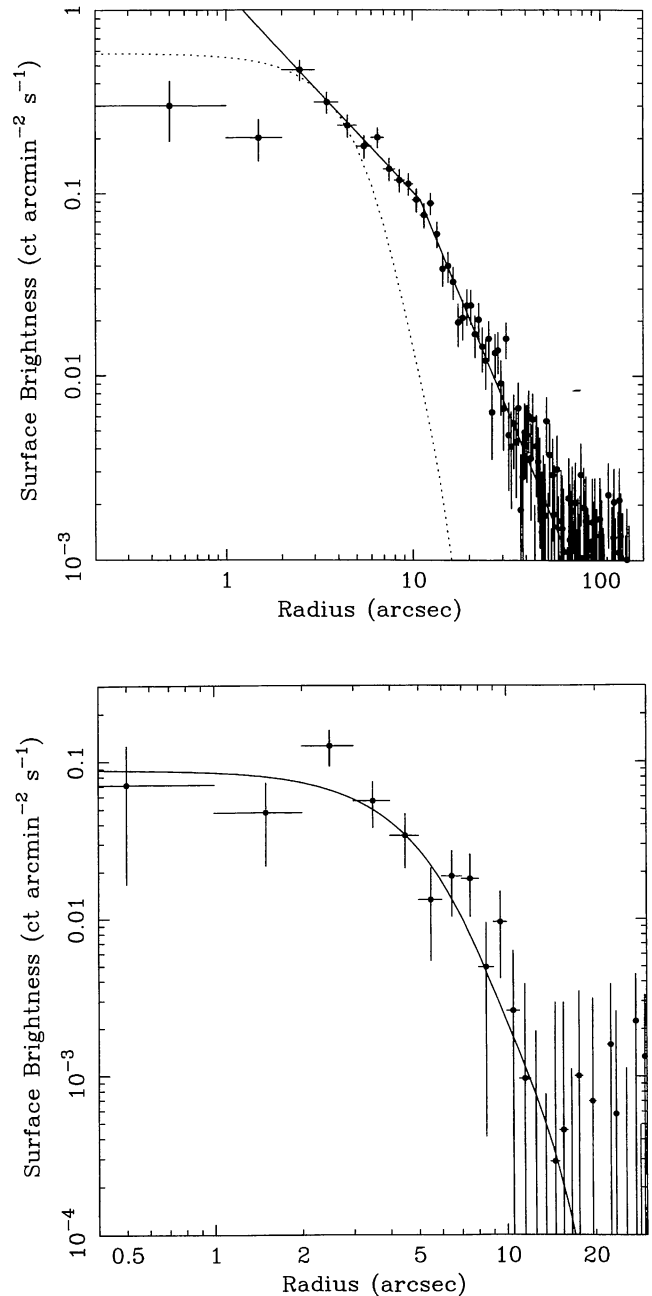

Figure 2. Top: surface brightness profile of the X-ray source associated with IRAS 09104 + 4109, after background subtraction. The dotted line shows the on-axis PSF of the HRI, and the solid line shows the best fit of a broken power law over 2–60 arcsec (with a break at $11.0^{+1.3}_{-1.1}$ arcsec, and slope of $1.1^{+0.1}_{-0.1}$ a smaller radii, $2.5^{+0.1}_{-0.1}$ at larger radii). Bottom: background-subtracted surface brightness profile of the second brightest source in the field, with the HRI PSF (solid line).

tred on IRAS 09104 + 4109, leading to a total exposure time of 7000 s, and an effective airmass of 1.132. The Loral 3 CCD was used with the O300 grism, leading to a wavelength coverage of 3980–9680 Å at a dispersion of 3 Å per pixel and a spectral resolution of ~ 11 Å. The spectral range and resolution of the observation are the same for all the field of view.
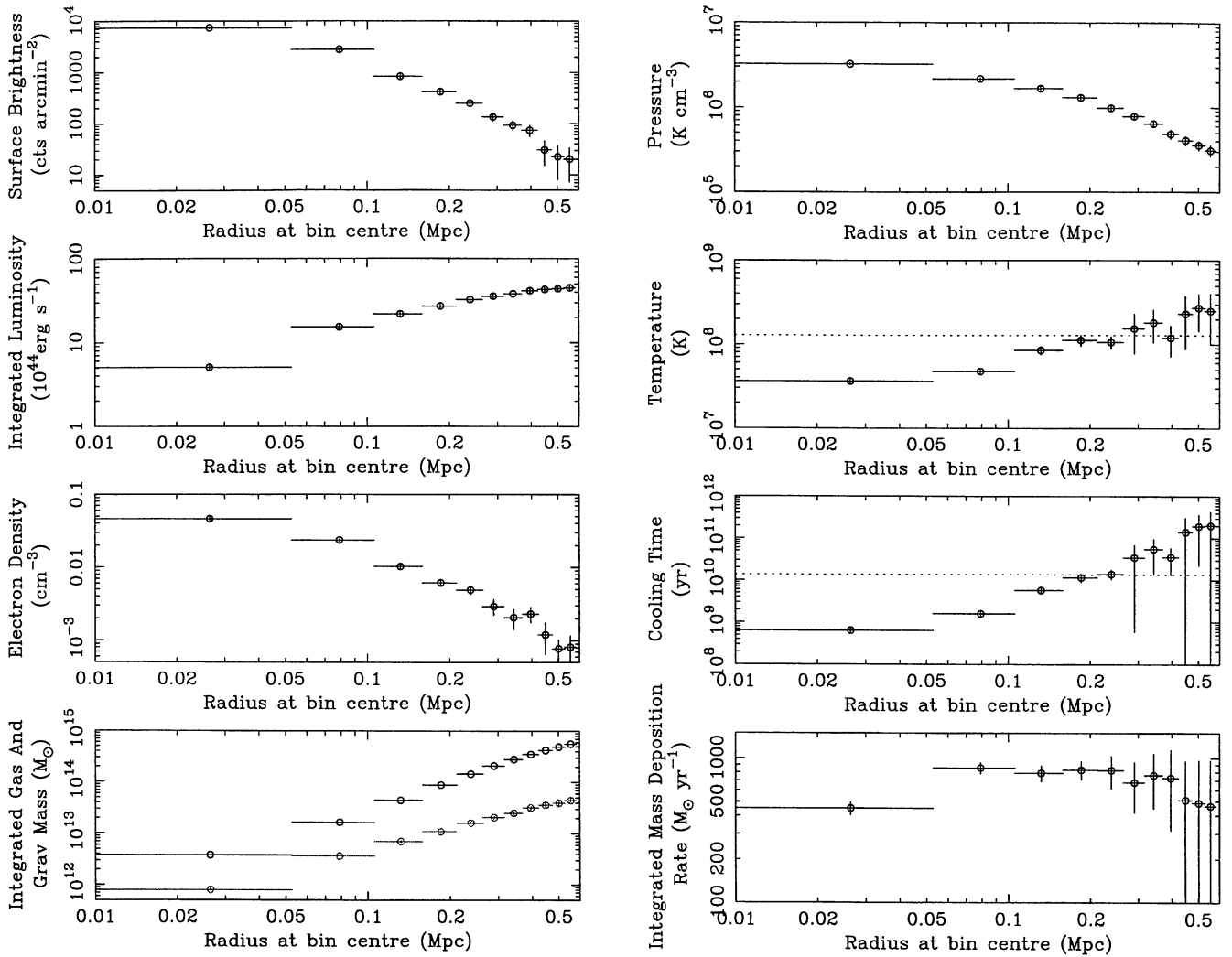
Figure 3. Radial profiles of the physical properties of the extended X-ray source of IRAS 09104 + 4109, from the deprojection analysis described in the text, assuming that the emission is due to thermal bremsstrahlung. The model shown indicates a massive cooling flow of $\sim 800 \, M_\odot \, yr^{-1}$, assuming no excess absorbing column density (see Section 2).

3.1   Data reduction

The data were reduced using an identical process to that described in detail for the quasar 3C 254 in CV96. In summary, the individual frames of IRAS 09104 + 4109 were each corrected for bad CCD columns, median-combined to remove cosmic ray events and then bias-subtracted. The frame was corrected for spatial distortion, flat-fielded using a normalized exposure of a tungsten lamp, and wavelength-calibrated using exposures of a neon-helium lamp. The data were flux-calibrated, corrected for atmospheric extinction, and for Galactic reddening, assuming A_V of 0.041 [the line-of-sight Galactic hydrogen column density was derived from Stark et al. (1992), and converted using the relation of Bohlin, Savage & Drake (1978), assuming R of 3.2 and the reddening law of Cardelli, Glayton & Mathis (1989)]. The data were then split into individual fibre spectra. Sky (and scattered-light) subtraction used a locally averaged spectrum from five or six sky fibres per row.

The final spectra suffer from the flux-calibration problem described in CV96, in that some flux is lost at wavelengths

beyond 6500 Å. The cause of this error is currently undergoing further investigation, and is not yet established. It is, however, easily corrected using observations of quasars taken during the same run, where the well-defined power-law slope of the nuclear continuum can be compared to high-quality/UV spectra in the literature (CV96). This simple systematic error has very little effect on the scientific conclusions derived from the data presented in this paper. The correction is the same for all fibres over the aperture and, were it inadequately made, would affect only the value of intensity ratios of emission lines widely separated in wavelength. The variation of these ratios across the aperture, and the morphology and distribution of these emission lines are unaffected.

Arc-lamp exposures were used to characterize fibre-to-fibre variations in the spectra output across the aperture, at the wavelengths of redshifted [O II] and [O III] (at ~ 5370 and ~ 7220 Å; the strongest emission lines of interest in IRAS 09104 + 4109). Variations across the aperture include a decrease in the instrumental resolution toward the edge of the aperture in the blue, and also slight systematic shifts in

line wavelength between fibres (CV96). The results of the arc-line fitting are used to remove these fibre systematics from the emission-line behaviour in the data for IRAS 09104 + 4109.

3.2 Emission-line fitting

The emission lines in the spectra from each fibre were fitted using QDP (Tennant 1991). QDP enables the construction of simple, yet physically realistic, models, where a small complex of neighbouring emission lines spanning a range of a few hundred Å, can be fitted together with a minimum of free parameters. Each line is fitted by a Gaussian with its centre, width and intensity as independent parameters. Narrow lines within a small complex are constrained to have the same velocity width as each other (there is no evidence for any broad components to the lines in IRAS 09104 + 4109), and to be at the same redshift. Additionally, lines with fixed intensity ratios (e.g. [O III] $\lambda\lambda 4959, 5007$ and [N II] $\lambda\lambda 6548, 6584$) have the relative ratios set. The continuum over this small wavelength range is most often adequately modelled as a constant.

Fitting the emission in IRAS 09104 + 4109 presents a further complication, as there is a second blueshifted component present in the main body of the galaxy (as noticed by K88). The blue component is typically shifted by -1250 km s^{-1} relative to the underlying system, and has 10–30 per cent of the flux in the main line. It is most clearly resolved in the Hβ + [O III] emission-line complex (Fig. 4). Thus, in addition to the combined fit to the main Hβ + [O III] (with four free parameters: the velocity shift, width and intensity of narrow Hβ and [O III] $\lambda 5007$), an additional complex is added. This blueshifted complex is characterised only by its relative intensity and velocity difference from the stronger

component; we assume the same velocity width and line ratio [O III]/Hβ as seen in the main component.

The bluer component seems to be present in all the strongest emission lines in the spectrum of IRAS 09104 + 4109, but resolving it in each fibre is less straightforward in lines other than the [O III], due either to the low line luminosity or to complications from doublets such as [N II] or [O II]. Modelling the Hα + [N II] complex is particularly problematic – not only is the spectrum much nosier in the red (Hα is redshifted to ~ 9460 Å), but any blueshifted component to Hα will be masked by the [N II] doublet lines (themselves possibly with blueshifted components). We do not attempt a rigorous fitting to this complex.

The galaxy continuum was also mapped in two featureless bands – in the blue (observed 5150 ± 150 Å, corresponding to the region between redshifted [Ne V] $\lambda 3346$ and [O II] $\lambda 3727$) and red (observed 7850 ± 150 Å, corresponding to just redward of the ~ 7600 Å atmospheric water absorption, and the [Fe II] $\lambda 5720$ emission line seen in the nucleus).

3.3 Results

The results from fitting all the spectra can be converted into 'images' of IRAS 09104 + 4109 (Fig. 5, opposite p. 1008), in the (line-free) continuum or the (continuum-free) emission-line intensity. Fig. 5 presents the reconstructed images of IRAS 09104 + 4109 in the continuum band, and in the intensity of the *main*, redder velocity component of the stronger emission lines. Due to the excellent seeing during the observation, all images (except the Hα image) peak in exactly the same fibre (i.e., within 0.4 arcsec of each other). The position of this fibre and its six immediately surround-
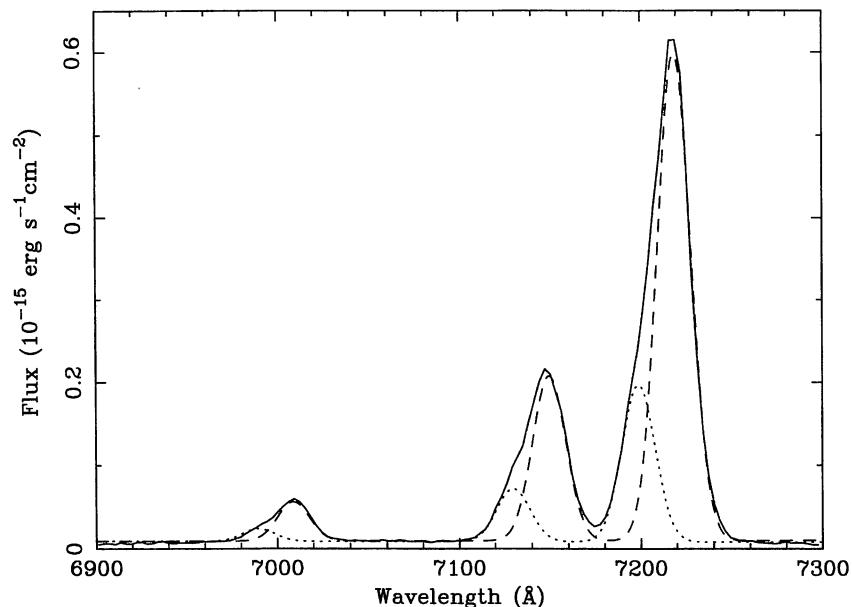

Figure 4. The spectrum of IRAS 09104 + 4109 around the [O III] + Hβ emission-line complex from the nuclear fibre, clearly showing the blue asymmetry to the lines (solid line). The two velocity components from the QDP model are decomposed into the main nebula (dashed line) and the blueshifted component (dotted line). The blueshifted component is fitted for this fibre as a relative offset of -1187 km s^{-1} from, and an intensity of 32 per cent of, the stronger, redder component.

ing fibres will be referred to in this paper as the 'nucleus' of the galaxy.

The comparatively low efficiency of ARGUS limits its practical use for study of the faint continuum of distant objects. The continuum images appear roughly symmetric, but only marginally extended, with FWHM of 1.1 ± 0.1 arcsec (B) and 1.2 ± 0.2 arcsec (R) along the row direction, and 0.9 ± 0.1 arcsec (B) and 1.0 ± 0.3 arcsec (R) perpendicular to the rows [FWHM of 0.9 and 0.7 arcsec respectively were measured for the blue continuum PSF in the quasar 3C 254 (CV96), from an adjacent exposure observed under similar seeing conditions]. The instrumental PSF of ARGUS is broader along the rows than in the perpendicular direction, due to resampling of the ARGUS output into MOS (CV96).

In the light of the emission lines, IRAS 09104 + 4109 is clearly extended, particularly to the north, where a bright emitting clump is embedded in the nebula, centred approximately 3 arcsec (23 kpc) north of the nucleus. The brightest region of this clump is resolved into an $\sim 2 \times 1.5$ arcsec^2 peak (15×11 kpc^2), elongated into a north–south plume toward the main body of the galaxy. Both this northern peak of emission and the nucleus are embedded in a larger envelope of line emission, extending out particularly to the north and east. At the detection level of this observation, the nebula does not extend out of the ARGUS aperture. We use a north–south cut for more detailed examination of the line-emission properties; this cuts through the major axis of the nebula, passing through both the northern emission-line peak, and the nucleus, as shown in Fig. 6. We show the normalized intensity of both [O III] and [O II] as a function of distance from the nucleus along this cut in Fig. 7.

The [O III] line intensity image of the blueshifted emission-line component is shown separately in Fig. 8 (opposite p. 1008), also demonstrating its spatial overlap with the main [O III] nebula. It is symmetric and centred on the same fibre as the underlying system (this is not an artefact of the fitting, as the relative intensity of the small component is a fully free variable). It follows the two-dimensional PSF of the instrument, so it is not resolved.

3.3.1 Line luminosity

IRAS 09104 + 4109 is a prodigious line-emitter, with total line luminosities of 1.5×10^{44} erg s^{-1} in [O III] $\lambda 5007$, 3.0×10^{43} erg s^{-1} in [O II], and 2.1×10^{43} erg s^{-1} in Hα. The central core contributes 75 and 50 per cent of the total luminosity in [O III] and [O II] respectively. The northern peak is brighter (compared to the nucleus) in [O II] than in [O III] (e.g. Figs 5 and 7; 12 and 7 per cent of the total flux, respectively), and is also clearly seen in the Hα, Hβ and [Ne III] $\lambda 3869$ emission-line images in Fig. 5. The blueshifted component has a total line luminosity of 3×10^{43} erg s^{-1} in [O III] and 2×10^{42} erg s^{-1} in [O II], so is itself exceptionally line-luminous.

3.3.2 Kinematic behaviour

Images can be constructed showing the kinematic behaviour of the emission lines deduced from the results of the line fitting. Maps of the FWHM of the main (red) component to the [O III] emission, and its radial velocity shift relative to

the nuclear fibre are presented in Fig. 9 (opposite p. 1008). In seven fibres the [O III] emission line is unresolved (the resolution varies across the aperture), and so for these fibres its linewidth was instead constrained to be the average of adjacent fibres. The fibres so affected are marked by dots the upper plot in Fig. 9. Plots of the velocity curve (relative to the nucleus) and FWHM of the [O III] along the major axis cut are shown in Fig. 10.

The velocity structure of this main component appears to vary smoothly across the entire nebula (Figs 9 and 10), although there is no obvious rotation. Across the main body of the galaxy the velocity gradient moves from a 200 km s^{-1} redshift in the south to a -100 km s^{-1} blueshift across the nucleus. Further north (including the embedded northern peak) the gas is again redshifted by a similar amount. There is also noticeable velocity width structure across the nebula which correlates with the velocity structure (both of which are independent parameters in the emission-line fitting). The narrowest line emission originates in the embedded northern peak. Where the line is blueshifted, it is also broader (Figs 9 and 10) to the north of the main body of the galaxy.

The blueshifted component to the line emission also shows a velocity tilt across its structure, similar to that seen in the main component, but with a slightly steeper gradient (226 ± 43 km s^{-1} per arcsec compared to 157 ± 23 km s^{-1} per arcsec for the redder component, over the central -1 to $+0.5$ arcsec region).

3.3.3 Ionization state

We map the ionization state of the main (redder) nebula in terms of the [O III]/[O II], [Ne III]/[O II] and [O III]/Hβ line intensity ratios in Fig. 11 (opposite p. 1008), and also plot the intensity ratio diagrams in Fig. 12. It is clear that there are dramatic changes in the ionization state across the nebula, most clearly demonstrated in the [O III]/[O II] map. The highest ionization region starts at a sharp edge ~ 0.8 arcsec north-east of the nucleus, and extends to the south-west of the nebula. The northern peak also shows up as slightly higher ionization lines evident in the nuclear spectrum. Similar ionization structure is seen in the maps of both [Ne III]/[O II] and [O III]/Hβ. The remaining diffuse nebula is at low ionization.

The measured value of Hα/Hβ is unreliable, due to the difficulties in resolving [N II], Hα and the blueshifted components of each at the noisier end of the spectrum. This ratio would also be the one most affected if the flux calibration correction was inadequate. We note, however, that the ratio shows no significant variation where measurable across the whole extended emission line region, and is consistent with Case B. An average spectrum from the seven fibres immediately on and around the position of the nucleus allows measurable ratios of [N II] $\lambda 6584$/H$\alpha \sim 0.5$ and [O I] $\lambda 6300$/H$\alpha \sim 0.16$.

We plot the line intensity ratios from the entire nebula in a diagnostic diagram in Fig. 12, along with the intensity ratios obtained from a slit spectrum in K88 for comparison (large open circles). Our line ratios are in good agreement with those found by K88, apart from the [O III]/Hβ ratio in the extended line emission. K88 state that a value for the [O III]/Hβ ratio around the northern peak is a factor of 2

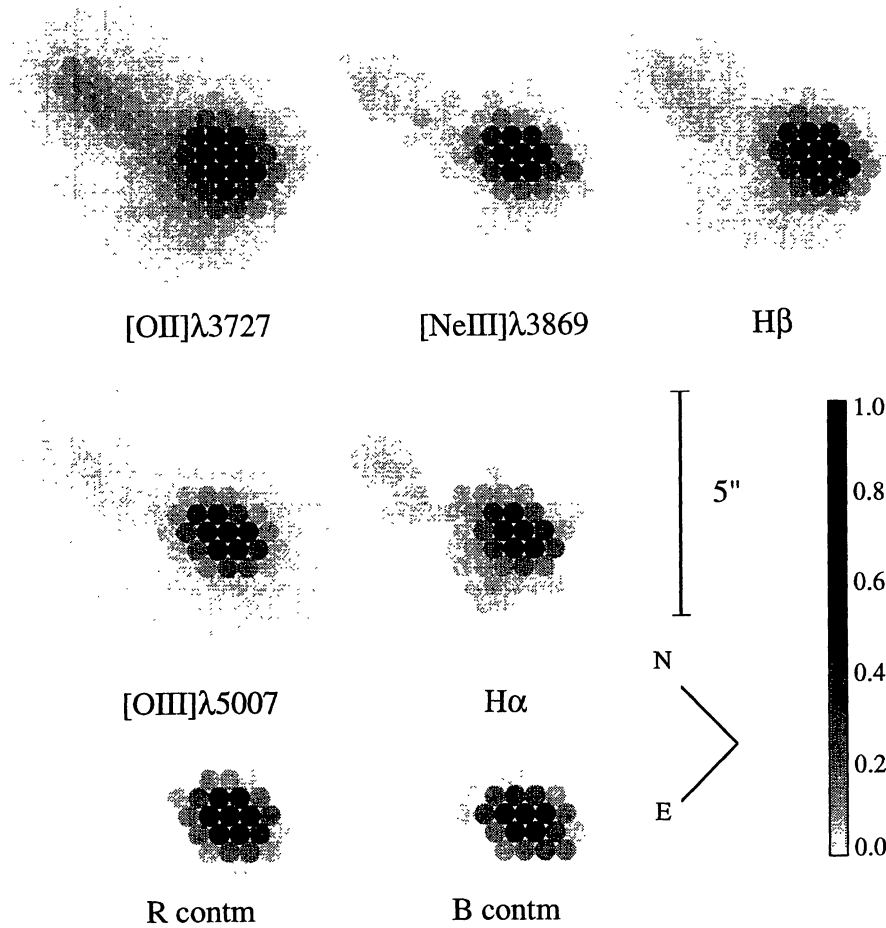[OII]λ3727 [NeIII]λ3869 Hβ

[OIII]λ5007 Hα

R contm B contm

Figure 5. Reconstructed images of IRAS 09104 + 4109 in the pure emission-line and continuum bands. The main (i.e., the redder) component to the emission-line fit only is shown in this figure. Where an emission line is detected in a spectrum, its intensity is represented by a grey-scale disc covering the position of that fibre in the hexagonal aperture. Where there is no detection, no disc is drawn for that fibre. The images are scaled such that the maximum intensity is black and zero is white, with the variation in grey-scale over this range shown by the colour bar. The range of values (in erg cm^{-2} s^{-1}) plotted are: (a) 1.8×10^{-17} to 1.5×10^{-15} for [O II]; (b) 1.2×10^{-17} to 1.1×10^{-15} for [Ne III]; (c) 1.0×10^{-17} to 1.1×10^{-15} for Hβ; (d) 1.7×10^{-17} to 13.6×10^{-15} for [O III]; (e) 6.1×10^{-17} to 1.8×10^{-15} for Hα; (f) 1.2×10^{-18} to 2.5×10^{-15} for the blue continuum; (g) 2.8×10^{-20} to 1.7×10^{-15} for the red continuum. Each image (except that in Hα) peaks in the same fibre. The aperture is oriented at a position angle of $-45°$, so north is the upper left-hand corner. Each fibre has a diameter of 0.4 arcsec (corresponding to 3 kpc at the redshift of IRAS 09104 + 4109).
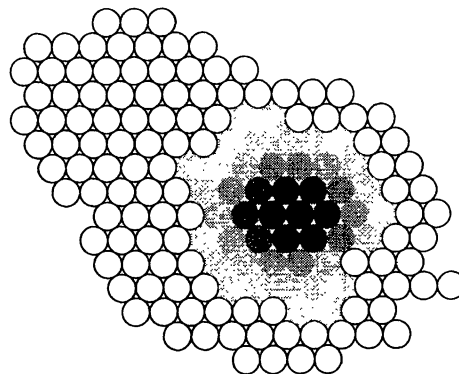
Figure 8. Intensity map of the [O III] line emission solely from the smaller, blueshifted component. The figure also demonstrates its spatial superposition on the main (redder) [O III] nebula (cf. Fig. 5). The peak intensity (black) is 4.3×10^{-15} erg cm^{-2} s^{-1}.
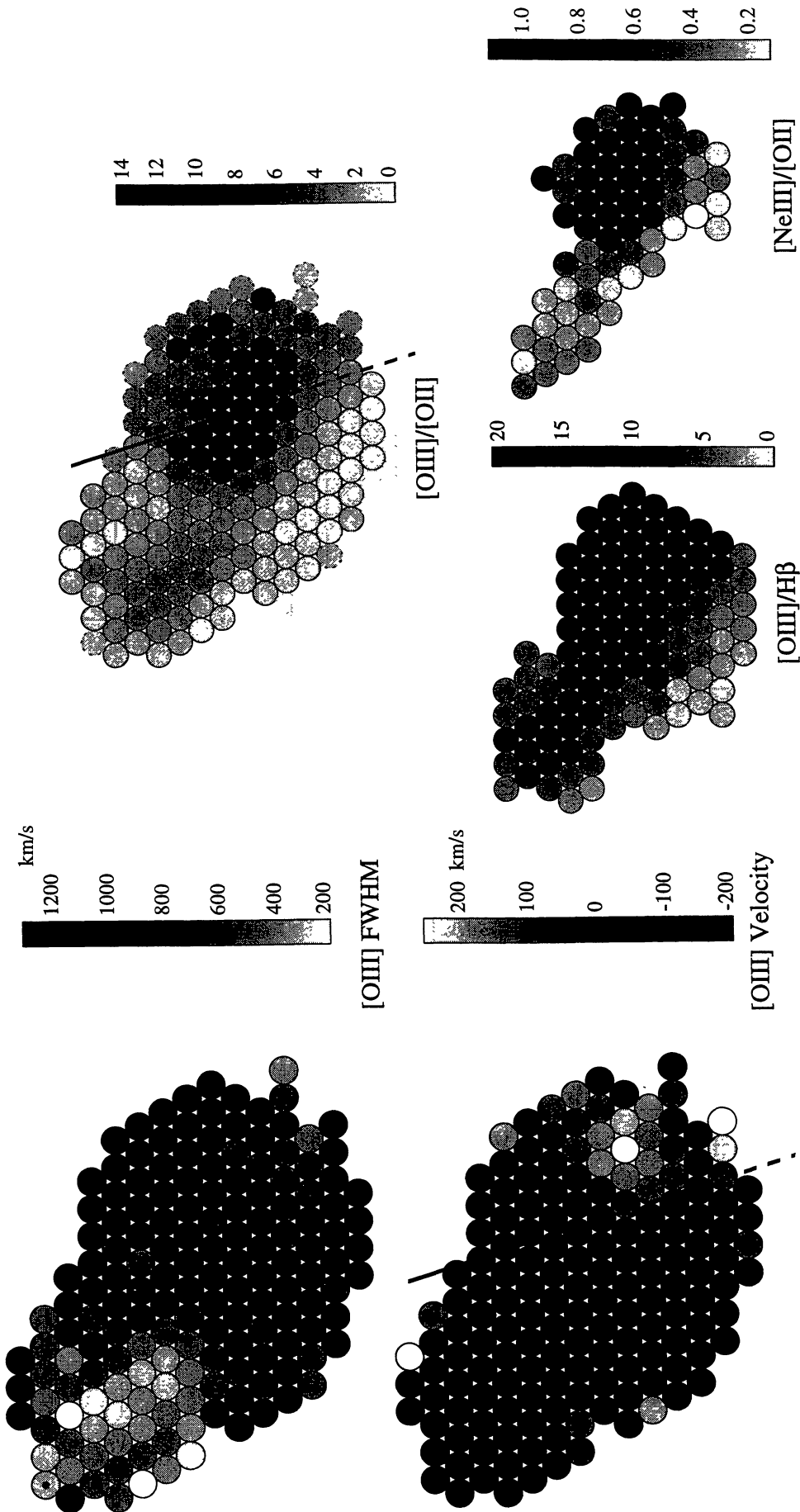
© 1996 RAS, MNRAS **283**, 1003–1014

Figure 9. Reconstructed images of IRAS 09104 + 4109 in the FWHM (top) and velocity relative to the nucleus (bottom) for the main (i.e., redder) component of the [O III] emission line. The asterisk represents the position of the nucleus, and fibres marked by a dot had the velocity width of the [O III] in their spectrum fixed, as described in the text. The solid line running at a position angle of 333° from north on the lower map marks the orientation of the radio source axis (HW93), assuming that the radio core lines up with the position of the nuclear fibre. The solid half of the line marks the jet side, and the dashed line the counterjet side, of the radio source.

Figure 11. The line intensity ratios of [O III]/[O II] (top), [O III]/Hβ (lower left) and [Ne III]/[O II] (lower right), with the relevant grey-scale to the right of each plot. The line intensity ratios plotted are for the main underlying component of emission only. Fibres are marked in the [O III]/Hβ and [Ne III]/[O II] plots only when both lines are detected in the spectrum. Fibres in the [O III]/[O II] plot (only) outlined by a broken line mark lower limits (i.e., where [O III] is detected and [O II] is not), and those fibre positions not outlined at all mark upper limits (where [O II] is detected but [O III] is not; mostly to the south-eastern edge of the nebula). The straight line in the [O III]/[O II] image again marks the axis of the radio source as in Fig. 9, and the position of the nucleus is marked by an asterisk in each map.

© 1996 RAS, MNRAS **283**, 1003–1014

higher than they find for the nuclear intensity ratio; we find instead that it is considerably less highly ionized than at the core of the galaxy, and assume that the true value they find is a factor of 2 *lower* than the nuclear ratio, and plot the ratio in the diagram accordingly. We mark the locus of shock- + precursor predictions (dotted line) for the shock velocities from 200 to 500 km s^{-1}, and a magnetic parameter $(B/n^{1/2})$ range of 0–4 G cm$^{-3/2}$ from Dopita & Sutherland (1995). Similarly, the solid line with pluses encompasses the

predictions of photoionization from the standard AGN continuum in CLOUDY, with ionization parameter U varying from -1 to -3.5, density ranging over $10^{0.5}$ to $10^{3.5}$ cm^{-3}, and assuming solar abundances (Ferland 1993).

In order to determine the average ionization state of the blue component, we sum the spectra from the nuclear fibres, and fit each emission line with the main component and a secondary component fixed at a shift of -1250 km s^{-1} (as determined from the [O III] fit). The blueshifted component of line emission (with ratios marked by open squares in Fig. 12) is at a slightly higher ionization than the main body of the nebula, but does not seem to occupy a distinct, different area in any of the diagrams. In the plot of [O II]/ [O III] versus [O III]/Hβ (Fig. 12), the blueshifted component and the central line ratios appear marginally more consistent with photoionization than with the shock loci [although shock models only up to 500 km s^{-1} are computed by Dopita & Sutherland (1995), and the size of the blueshift, if entirely kinematic, suggests shock velocities much greater than this]. Further off-nucleus, the ionization drops and the line ratios are consistent with either loci, until at larger radii an increasing contribution from Hβ takes the ratios more into the shock-heated regime. The situation remains ambiguous in other line ratio plots, such as those suggested to be good discriminators between shock and photoionization models (e.g. Clark & Tadhunter 1996). Unfortunately, these plots rely on lines such as He II or [O III] $\lambda4364$ that are only measurable close in to the central nucleus, and both ionization models appear equally consistent with the observed line ratios in this region.

A further indication for shock-ionization is if the dynamics of the gas is related to its ionization state (Baum, Heckman & van Breugel 1992; Crawford & Fabian 1992; Dopita & Sutherland 1995). We find no obvious relation-
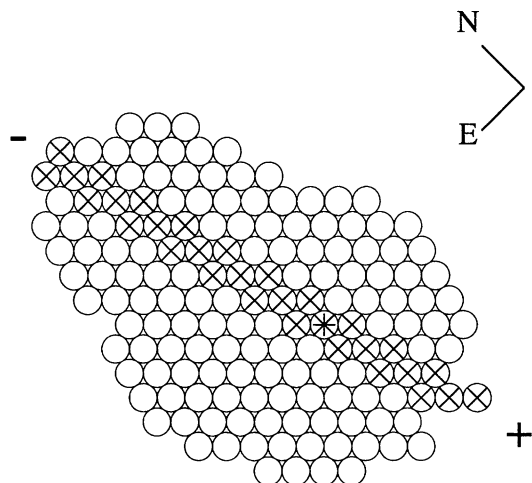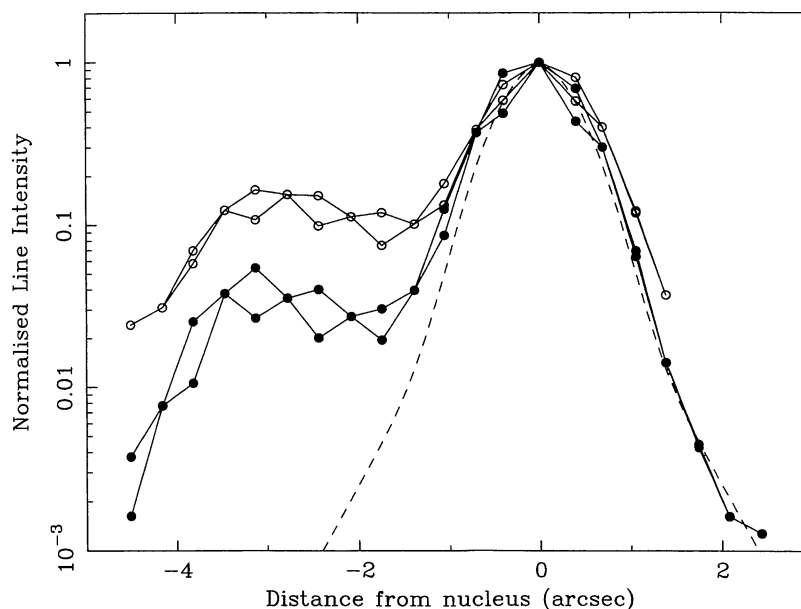

Figure 6. Outline of the fibres where [O III] line emission is detected (cf. the [O III] image in Fig. 5). Fibres marked by a diagonal cross are those whose spectra to construct the north–south cut used for detailed examination in this paper and in Figs 7 and 10. The cut passes through the nuclear fibre (indicated by an asterisk), and the ' − ' and ' + ' symbols mark the directional sense of the axes assumed in the cuts.

Figure 7. Intensity profile of the main (i.e., redder) component of the [O II] (open circles) and [O III] (filled circles) line emission along the major axis of the nebula, using the fibres shown in Fig. 6. Negative distances (to the left) are north, and positive distances south, of the nucleus, and the line intensities have been normalized to one in the nuclear fibre. The instrumental PSF is shown by the dashed line, with the worst-case FWHM of 0.9 arcsec (i.e., along the rows). Alternate distances are double-valued, because there are two fibres along the cut corresponding to the same radius (see Fig. 6).
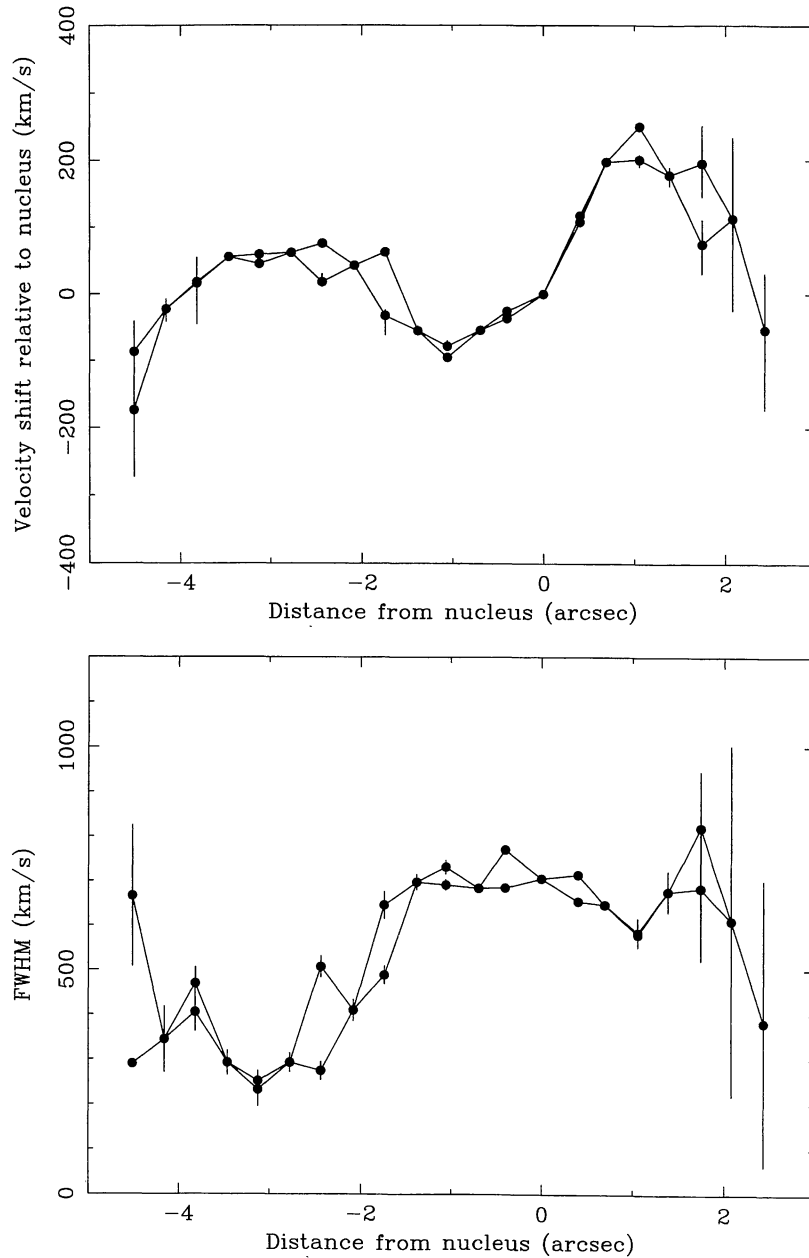
Figure 10. Velocity of the main component of [O III] relative to the nucleus (upper panel) and its FWHM (lower panel) along the major axis cut shown in Fig. 6. Error bars are 1σ errors from the fitting alone, and do not encompass any systematics from the data reduction.

ship between the kinematics of the gas (its FWHM) and its ionization state (measured by [O III]/Hβ) or Hβ line flux. In particular, we do not find the v^3 relationship predicted (CF92; Dopita & Sutherland 1995) if shocks are responsible for powering the diffuse envelope of extended emission (i.e., away from the northern peak and the nucleus). For a given linewidth, however, both the northern peak and the nucleus show an enhanced Hβ flux and ionization state.

3.3.4   *Summary and optical observations*

IRAS 09104 + 4109 is only marginally extended in the continuum, but the observation is not sufficiently sensitive to detect faint extended continuum.

The line emission of IRAS 09104 + 4109 is extended, with a particular enhancement forming a 3-arcsec-long plume to the north of the main body of the galaxy. Both this and the nucleus are embedded in general diffuse envelope of emission. The line emission has a second, blueshifted component spatially centred around the nucleus, and offset by -1300 km s^{-1}.

The velocity structure in the main nebula is redshifted to either side of the nebula, with a slight blueshift to the northern edge of the nucleus. The velocity width structure correlates with the velocity shift, in that the emission lines are broader where they are blueshifted.

The main nebula shows variations in its ionization state, with the blueshifted component, the nucleus and the
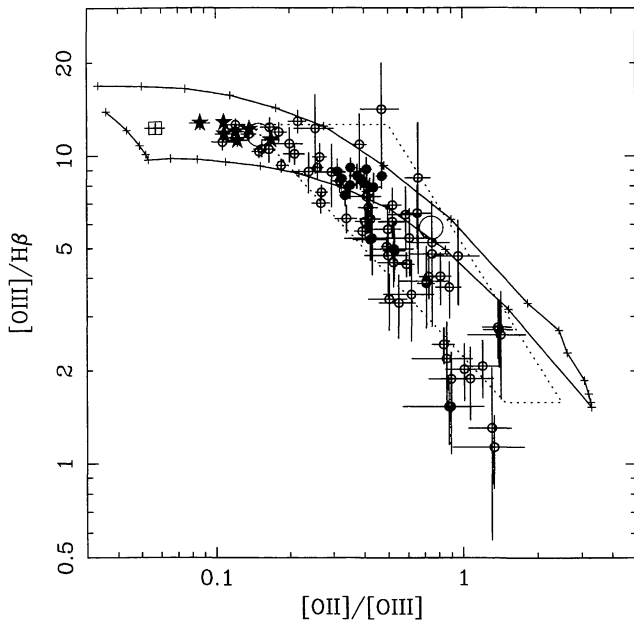
Figure 12. Line-intensity ratio diagram for [O II]/[O III] versus [O III]/Hβ for all points where all lines are measured in the nebula. Star symbols mark the ratios from the nuclear fibres, filled circles the ratios at the position of the northern peak, and open circles the ratios for the rest of the nebula. The open square marks the line ratios in the blueshifted component, and the two large open circles mark the values taken from K88 (and assuming a factor of 4 error from the value of [O III]/Hβ quoted for the extended line emission; see text for details). The solid line (and 'plus' marks) encloses the locus predicted for a simple power-law photoionization model in CLOUDY of varying ionization parameter U over the range -1 to -3.5, varying density over the range of 3 to 3000 cm^{-3} and solar abundance. The dotted line encloses the range of predictions from shock models of velocity varying over 200 to 500 km s^{-1} from Dopita & Sutherland (1995).

northern peak all at a higher ionization state than the rest of the nebula. The line ratios for the extended gas do not discriminate totally between the predictions of shock and photoionization, although they could be interpreted as photoionization dominating at the centre, and shock ionization becoming increasingly important at larger radii.

There is no obvious proportionality between the line-width and either the Hβ flux or [O III]/Hβ where the line ratios suggest that shock ionization may be important.

4 DISCUSSION

4.1 The nebula and northern emission peak

The 'secondary peak' in the line emission centred 3 ± 1 arcsec north of the nucleus (Fig. 5; K88) is evident as an elongated extension to the central body of the galaxy in the R-band image of HN88. Our ARGUS observation is not sufficiently sensitive to detect any extended continuum emission at this position. Given the very high equivalent width of the redshifted [O III], however, which lies at the peak of the R-band response, we suspect that the R-band extension of HN88 is caused almost entirely by emission-line contamination.

The northern peak forms a simple enhancement within the large extended emission-line region around the main galaxy; there are no abrupt changes in the intensity distribution or ionization state between this component and the galaxy (Figs 5 and 12). There is, however, a marked change in the velocity structure (both in relative velocity and FWHM) at the 'edge' between the main nebula and the northern peak (Fig. 9) occurring between four and five fibres (~ 1.8 arcsec) north of the central fibre, suggesting that this extension is physically separate. The dipolar velocity curve of the main body of the nebula can be interpreted as simple rotation about an east–west axis, misaligned by approximately 35° from the radio source axis. The northern extension is at a relative redshift of only ~ 100 km s^{-1} with respect to the nucleus. Although its elongated morphology is suggestive of a gas cloud merging with the cD galaxy, its very low relative velocity precludes it being in either rotation or free-fall around the main galaxy. [Velocity dispersion within a cD galaxy are typically above 250 km s^{-1}, and the measured dispersion of globular clusters surrounding each of M87, the central galaxy in the Virgo cluster, and NGC 1399, the central galaxy in the Fornax cluster, is around 390 ± 50 km s^{-1}: (Mould et al. 1990; Grillmair et al. 1994).] An additional difficulty for the merger interpretation for IRAS 09104 + 4109 is the very survival against ram-pressure stripping of any gas-rich system falling into the core of this very rich cluster, whereas the cooling flow is probably continually supplying this region with cooled gas. The extended line-emitting gas in IRAS 09104 + 4109 is thus essentially static with respect to the central cluster galaxy, and the northern peak is most likely to be a local enhancement of gas density provided by, and confined in palce by, the strong cooling flow.

K88 identified the northern peak of line emission as the region of the highest ionization in the system, stating an [O III]/Hβ intensity ratio a factor of 2 larger than that observed in the nucleus. We find this to be incorrect (see Section 3.3.4), and that the highest ionization region is clearly around, and to the south-west of, the nucleus. The northern peak does, however, seem to be at anomalously high ionization (and luminous in Hβ) for its velocity width. HW93 identified it as a possible ionization 'cone', analogous to those commonly seen in Seyfert 2 galaxies (Pogge & De Robertis 1993). The rationale for this identification was the orientation of the northern peak in a direction perpendicular to the measured position angle of the polarization, as well as the extraordinarily high ionization state given by K88. It is peculiar, then, that it appears so misaligned with, and asymmetric around, the radio source axis (HW93; Fig. 11). We note that the other region of higher ionization (apart from the nucleus) is located to the directly opposing side of the nucleus. If the identification were correct, and cones of ionizing radiation are escaping from the nucleus along a north–south axis; this axis is perpendicular to any rotational axis within the main part of the nebula. Line-intensity diagrams suggest that power-law ionization may dominate around the nucleus and the northern peak, but that the rest of the extended line emission is powered by other means. There is no obvious relation between the kinematics of the line emission and its ionization state over the nebula, suggesting that it may well not be simple shock ionization.

4.2   The central quasar

The optical properties of IRAS 09104 + 4109, such as its emission-line spectrum, highly polarized continuum, and lack of broad Balmer line components are characteristic of a Seyfert 2 type nucleus (K88). The host galaxy of IRAS 09104 + 4109 is a giant elliptical, quite unlike the spiral galaxies usually hosting Seyfert nuclei, and although a broad component to Mg II is seen in the nuclear spectrum (HW93), there is as yet no evidence for broad lines seen in scattered light. The IR luminosity of IRAS 09104 + 4109, however, is more comparable to those of similar-redshift QSOs (and it is, in fact, classified as such by HN88). There is little evidence for any X-ray emission from the nucleus, so the emission from any quasar at the core of the galaxy must be highly absorbed along the direct line of sight. This has led to the suggestion that IRAS 09104 + 4109 represents a new population of 'type 2 quasars'; i.e., Seyfert 2 galaxies emitting at quasar luminosities (Fabian et al. 1994). This putative class of highly obscured quasars might also include other hyperluminous *IRAS* galaxies such as IRAS F15307 + 3252 (Fabian et al. 1996).

From the deprojection of the X-ray data, we can extrapolate the measured pressure profile into the core of the cluster to estimate a pressure of $(3.6$–$4.3) \times 10^6 \, cm^{-3} \, K$ at a radius of 2.8 arcsec, compatible to the projected radius of the northern peak (the pressure inferred increases with the amount of excess intrinsic absorption allowed in the X-ray deprojection). Assuming that the gas in this region is photoionized by a standard AGN continuum, we match the [O III]/Hβ, [O III]/[O II] intensity ratios and the inferred X-ray pressure to predictions from CLOUDY. We find an excellent match of the observed line ratios to a model with density $180 \, cm^{-3}$, ionization parameter U of $10^{-2.64}$, predicting a gas pressure of $3.9 \times 10^6 \, cm^{-3} \, K$. [Other models in the density range 100 to $180 \, cm^{-3}$, ionization parameter $10^{-2.6}$ to $10^{-2.7}$, are all compatible with the small range of line ratios, predicting slightly lower gas pressures of $(2.1$–$3.8) \times 10^6 \, cm^{-3} \, K$.] The total energy in the ionizing continuum (between $10^{-4} \, eV$ and 100 MeV) inferred from this 'best' model is $10^{46.86} \, erg \, s^{-1}$, agreeing well with the total luminosity of $2.4 \times 10^{13} \, L_\odot$ ($10^{46.96} \, erg \, s^{-1}$) measured for IRAS 09104 + 4109 at rest-frame wavelengths between 0.3 and 70 μm (K88).

4.3   A central cavity

Given its exact alignment with, and symmetric distribution about, the nucleus, the most plausible explanation of the secondary blueshifted component in the line emission is that it is due to an outflow of gas originating at the galaxy nucleus. It is thus especially intriguing that the X-ray source associated with IRAS 09104 + 4109 shows a dip in its surface brightness profile in the innermost 2-arcsec radius (consistent with the PSF of the *ROSAT* HRI; FC95).

4.3.1   A superwind

Broad, blueshifted asymmetric emission-line profiles are common in low-redshift *IRAS* galaxies selected to be bright in the far-infrared (Armus, Heckman & Miley 1989), and are interpreted as a starburst-induced supernova wind

(Heckman, Armus & Miley 1990). The line emission is then emitted from shock-heated ambient gas swept up in a thin skin on a bubble inflated by the outflow. The line ratios in the blueshifted component of IRAS 09104 + 4109 seem more compatible with power-law photoionization than with shocks, although the shock models plotted in Fig. 12 are computed only up to velocities of 500 km s^{-1}, whereas the blueshift suggests an outflow velocity around twice this value.

In this interpretation, the redshifted line emission from the far side of the bubble is assumed hidden by dust obscuration. In the case of IRAS 09104 + 4109, however, the dust appears to be confined to a small cocoon around the nucleus rather than mixed in with the nebula (K88; HW93), suggesting instead an anisotropic cavity. A supernova-inflated bubble would be filled by hot supernova ejecta, which, if emitting at temperatures above $10^8 \, K$, would not necessarily be detectable in our *ROSAT* HRI image, thus accounting for the deficit of observed X-rays in this region. The pressure measured from the [S II] lines in the far-infrared-selected galaxies imply that such superbubbles can generate pressures of more than $2 \times 10^6 \, cm^{-3} \, K$ over regions 1–10 kpc in diameter, and typically $> 2 \times 10^7 \, cm^{-3} \, K$ at the centre. Thus it is feasible that the starburst could form within the high-pressure environment we infer from the X-ray data. The radio source in IRAS 09104 + 4109 has an unusually bright core, given that its jet–counterjet ratio implies that the source lies close to the plane of the sky (HW93). However, if there is a contribution from radio-emitting synchrotron plasma within the superbubble, this could account for the anomalously bright core.

4.3.2   The radio source

Alternatively, the X-ray 'hole' could be due to the displacement of the cooling flow gas by the expansion of inner parts of the radio structure. Such cavities are seen as similar holes in the X-ray surface brightness around the inner 18 kpc region of 3C 84, the radio source at the centre of the Perseus cluster, which has a $\sim 300 \, M_\odot \, yr^{-1}$ cooling flow (Böhringer et al. 1993). Although the central galaxy (NGC 1275) has a luminous, extended emission-line nebula, there are no obvious coincidences between the X-ray holes and the spatial distribution, velocity profiles or kinematics of the optical gas.

As well as having an anomalously bright radio core for its apparent inclination, IRAS 09104 + 4109 is an exception to the alignment of the radio source structure with the optical polarization axis seen in other high-luminosity radio galaxies at intermediate redshift (Tadhunter et al. 1992; HW93). These arguments, along with the identification of the northern peak as a high-ionization cone, led HW93 to suggest that a recent change in radio jet direction has occurred, with the nuclear jet now decoupled from the large-scale radio structure and beamed at a smaller angle of inclination. If such a recent change of behaviour had taken place, the new jet may be responsible for pushing fresh cavities in the X-ray gas. Whilst this change in radio source direction would account for the unusually bright radio core, there is no obvious evidence for precession of the radio jets in the shape of the extended structure of the radio source. In this

interpretation, the blueshifted component is assumed to be ionized by fast shocks generated by the radio jets stirring up turbulence in the central regions of the cluster. Unless the jet is oriented much along our line of sight, there is less reason for the resulting cavity and outflow to be so spatially symmetric around the nucleus.

As we do not spatially resolve the blueshifted component, we are unable to discriminate between possible origins on energetic grounds. Correct interpretation of the central cavity requires high-resolution radio images of the direction and structure of the radio source in the core.

4.4 The cooling flow

The full HRI exposure confirms that the X-ray source associated with IRAS 09104 + 4109 is spatially extended on a scale of a few hundred kiloparsecs, and thus that the bulk of the X-ray emission cannot originate from a point source. The X-ray surface brightness profile is typical of that seen in nearby cooling flow clusters: $\propto r^{-1}$ within a core where cooling is important, and $\propto r^{-2}$ or steeper at larger radii. The break in the power-law model is at ~ 85 kpc, smaller than, but not inconsistent with, the results from the deprojection analysis, which shows mass deposition is taking place, mostly within the central two bins (< 110 kpc). The deprojection analysis suggests a larger cooling radius of ~ 250 kpc; within this radius the cooling time of the gas is less than the Hubble time at this redshift (1.4×10^{10} yr). The discrepancy between the cooling radius and the radius within which the bulk of the mass deposition is occurring is similar to other cluster cooling flows, such as that around Cygnus A. This behaviour may indicate that the cluster suffered a disruption, such as that due to a major cluster–cluster merger, and that most of the present cooling flow has developed over the last 2×10^9 yr (Reynolds & Fabian 1996). The X-ray properties of the cluster around IRAS 09104 + 4109 are very similar to those of three X-ray-selected clusters at almost comparable redshift, A1835 ($z = 0.252$), Z3146 ($z = 0.291$) and E1455 + 223 ($z = 0.258$), with mass deposition rates of ~ 2300, ~ 1400 and ~ 1500 $M_\odot$ yr^{-1} respectively (Allen et al. 1996).

4.5 Interrelation of the quasar and cooling flow

Many lower redshift cooling-flow central cluster galaxies also have extended emission-line nebulae on scales of 5–20 kpc (Heckman et al. 1989, and many references therein; Crawford & Fabian 1992). The most luminous of these nebulae [$L(\mathrm{H}\alpha) \sim 10^{40.5} - 10^{42.5}$ erg s^{-1}] are those associated with the stronger cooling-flow clusters ($\dot{M}$ of a few hundred $M_\odot$ yr^{-1}), and usually with a strong radio source in the central galaxy. The Hα luminosity from IRAS 09104 + 4109 (2.1×10^{43} erg s^{-1}) is comparable to that of the most line-luminous cooling flow known, Z3146 at $z = 0.29$ which has a (long-slit) Hα luminosity $\sim 10^{43}$ erg s^{-1}. Both the velocity curve and velocity widths (Figs 9 and 10) along the major axis of the nebula of IRAS 09104 + 4109 are also similar to those properties in the more luminous cooling-flow clusters (e.g., the kinematics of the nebula in A2597; Crawford & Fabian 1992). Despite sharing these characteristics of massive cooling-flow systems, its higher ionization nuclear spectrum, the presence of very high-ionization lines such as

those from He II, [Ne V] and [Fe VII], extreme IR luminosity (a factor of 30 higher than the most IR-luminous cooling-flow system previously known, A1068; Allen et al. 1995) and the presence of a polarized optical continuum mark IRAS 09104 + 4109 out as subtly different. All these differences from low-redshift cooling-flow systems can be accounted for by the presence of a quasar at the core of the galaxy. Indeed, our photoionization modelling for the northern peak suggests that an ionizing luminosity of around 10^{47} erg s^{-1} is required, typical of luminous quasars. The relative importance of a starburst component in addition to a central AGN in the galaxy core remains ambiguous. We do not have a high enough signal-to-noise ratio in the galaxy spectrum to test whether the excess blue continuum is extended, although we note that its PSF is similar to that of the red continuum, which might suggest a stellar origin rather than a point source following the instrumental PSF.

IRAS 09104 + 4109 is the best (i.e., directly proven from the X-ray image) case yet known for a cooling flow to be occurring around a quasar. Indirect evidence for the presence of a cooling medium around radio-loud quasars has been found from the high pressures inferred within the extended emission-line regions (assuming that the quasar continuum is the major source of ionization; Crawford & Fabian 1989; Forbes et al. 1990; CV96). It has been claimed that the central activity in IRAS 09104 + 4109 is being fuelled by a tidal interaction with a small companion galaxy (HN88), but were this to be happening, it is within the confines of one of the most massive cooling flows known. We find no evidence that the gas in the nebula is in either rotation or free-fall toward the central cD galaxy, instead forming a large, relatively static system at the cluster core. Alternatively, only a tiny fraction of the X-ray inferred mass deposition rate need reach the central active nucleus to fuel the quasar activity at the core (Fabian et al. 1986; Fabian & Crawford 1990). If the cooling flow were responsible for fuelling the quasar, it has been proposed that the disruption due to merging of subclusters to form rich clusters may either misdirect or temporarily cut off this supply and cause the demise of the luminous quasar activity (Fabian & Crawford 1990). The quasar in IRAS 09104 + 4109 lies in a very rich environment, one that possibly suffered a major disruption over 2×10^9 yr ago, as is hinted in the X-ray deprojection results.

5 CONCLUSIONS

From most of its distinguishing features – such as its radio and mid-IR luminosity, ionization state, clustered environment, and extended emission-line nebula – IRAS 09104 + 4109 appears to host a comparatively ordinary quasar, albeit one suffering from an enormous level of central obscuration that completely blocks the broad-line region and optical and X-ray nucleus from our line of sight. It may thus be a member of the long-sought class of 'type 2' quasars. Fortuitously, the heavy central obscuration has allowed us to examine its immediate environment in unprecedented detail for a quasar. A long pointed *ROSAT* HRI observation has confirmed that IRAS 09104 + 4109 lies at the centre of a massive cooling flow, with an integrated mass deposition rate of 800–1100 $M_\odot$ yr^{-1}. This is

the first X-ray-detected cooling flow around a quasar, and supports the findings of other less direct methods of investigation that have inferred strong cooling flows to be occurring around intermediate-redshift quasars. The central galaxy is surrounded by an extensive emission-line nebula, encompassing a secondary peak of emission which we identify as a possible ionization cone, although it is not aligned along the radio source axis. The kinematics of the ionized gas suggest that the nebula forms a large, relatively static system at the cluster core, and is unlikely to be accreting further on to the galaxy. The variation of line-intensity ratios across the nebula suggests that photoionization is important at the nucleus and ionization cone, but that other ionization sources such as shocks may dominate at larger distances; however, we do not find the expected relationships expected from shock-ionization, between the ionization state or flux of the ionized gas with its kinematic structure. The emission-line profiles around the nucleus show a highly blueshifted, highly ionized component of ionized gas that probably comprises some kind of nuclear outflow, caused by either the central radio source or a massive supernova wind. Such an outflow may also be responsible for the dip in surface brightness seen at the centre of the X-ray source.

ACKNOWLEDGMENTS

REFERENCES

Allen S. W., Fabian A. C., Edge A. C., Böhringer H., White D. A., 1995, MNRAS, 275, 741
Allen S. W., Fabian A. C., Edge A. C., Bautz M. W., Furuzawa A., Tawara Y., 1996, MNRAS, 283, 263
Armus L., Heckman T. M., Miley G. K., 1989, ApJ, 347, 727
Baum S. A., Heckman T. M., van Breugel W., 1992, ApJ, 389, 208
Bohlin R. C., Savage B. D., Drake J. F., 1978, ApJ, 224, 132
Böhringer H., Voges W., Fabian A. C., Edge A. C., Neumann D. M., 1993, MNRAS, 264, L25
Cardelli J. A., Clayton G. C., Mathis J. S., 1989, ApJ, 345, 245
Clark N. E., Tadhunter C. N., 1996, in Carilli C. L., Harris D. E., eds, Cygnus A – Study of a Radio Galaxy. Cambridge Univ. Press, Cambridge, p. 15
Crawford C. S., Fabian A. C., 1989, MNRAS, 239, 219
Crawford C. S., Fabian A. C., 1992, MNRAS, 259, 265
Crawford C. S., Vanderriest C., 1996, MNRAS, in press (CV96)
Dopita M. A., Sutherland R. S., 1995, ApJ, 455, 468
Ebeling H., White D. A., Rangarajan F. V. N., 1996, MNRAS, in press
Eisenhardt P. R., Armus L., Hogg D. W., Soifer B. T., Neugebauer G., Werner M. Q., 1996, ApJ, 461, 72
Fabian A. C., Crawford C. S., 1990, MNRAS, 247, 439
Fabian A. C., Crawford C. S., 1995, MNRAS, 274, L63 (FC95)
Fabian A. C., Arnaud K. A., Nulsen P. E. J., Mushotzky R. F., 1986, ApJ, 305, 9
Fabian A. C. et al., 1994, ApJ, 436, L51
Fabian A. C., Cutri R. M., Smith H. E., Crawford C. S., Brandt W. N., 1996, MNRAS, in press
Ferland G. J., 1993, University of Kentucky Department of Physics and Astronomy Internal Report, University of Kentucky
Forbes D. A., Crawford C. S., Fabian A. C., Johnstone R. M., 1990, MNRAS, 244, 680
Frogel J. A., Gillett F. C., Terndrup D. M., Vader J. P., 1989, ApJ, 343, 672
Grillmair C. J., Freeman K. C., Bicknell G. V., Carter D., Couch W. J., Sommer-Larsen J., Taylor K., 1993, ApJ, 422, L9
Heckman T. M., Baum S. A., van Breugel W. J. M., McCarthy P., 1989, ApJ, 338, 48
Heckman T. M., Armus L., Miley G. K., 1990, ApJS, 74, 833
Hines D. C., Wills B. J., 1993, ApJ, 415, 82 (HW93)
Hutchings J. B., Neff S. G., 1988, AJ, 96, 1575 (HN88)
Kleinmann S. G., Hamilton D., Keel W. C., Wynn-Williams C. G., Eales S. A., Becklin E. E., Kuntz K. D., 1988, ApJ, 328, 161 (K88)
Liu M., Graham J., Wright G., 1996, ApJ, submitted
Mould J. R., Oke J. B., de Zeeuw P. T., Nemec J. M., 1990, AJ, 99, 1823
Pogge R. W., De Robertis M. M., 1993, ApJ, 404, 563
Reynolds C. S., Fabian A. C., 1996, MNRAS, 278, 479
Soifer B. T., Neugebauer G., Armus L., Shupe D. L., 1996, AJ, 111, 649
Stark A. A., Gammie C. F., Wilson R. W., Bally J., Linke R. A., Heiles C., Hurwitz M., 1992, ApJS, 79, 77
Tadhunter C. N., Scarrott S. M., Draper P., Rolph C., 1992, MNRAS, 256, 53P
Tennant AF, 1991, NASA Technical Memorandum 4301
Vanderriest C., 1995, in Comte G., Marcelin M., eds, ASP Conf. Ser. 71, Tridimensional Optical Spectroscopic Methods in Astrophysics. Astron. Soc. Pac., San Francisco, p. 209
White D. A., 1996, MNRAS, submitted